Supplementary Information

Cyanogel-Enabled Homogeneous Sb–Ni–C Ternary Framework Electrodes for Enhanced Sodium Storage

Ping Wu,[†,‡] Anping Zhang,[‡] Lele Peng,[†] Fei Zhao,[†] Yawen Tang,[‡] Yiming Zhou,[‡] and Guihua Yu,[*,†]

[†]Materials Science and Engineering Program and Department of Mechanical Engineering, The University of Texas at Austin, Austin, Texas 78712, United States

[‡]Jiangsu Key Laboratory of New Power Batteries, Jiangsu Collaborative Innovation Center of Biomedical Functional Materials, School of Chemistry and Materials Science, Nanjing Normal University, Nanjing 210023, China

*E-mail: ghyu@austin.utexas.edu (G.Y.).

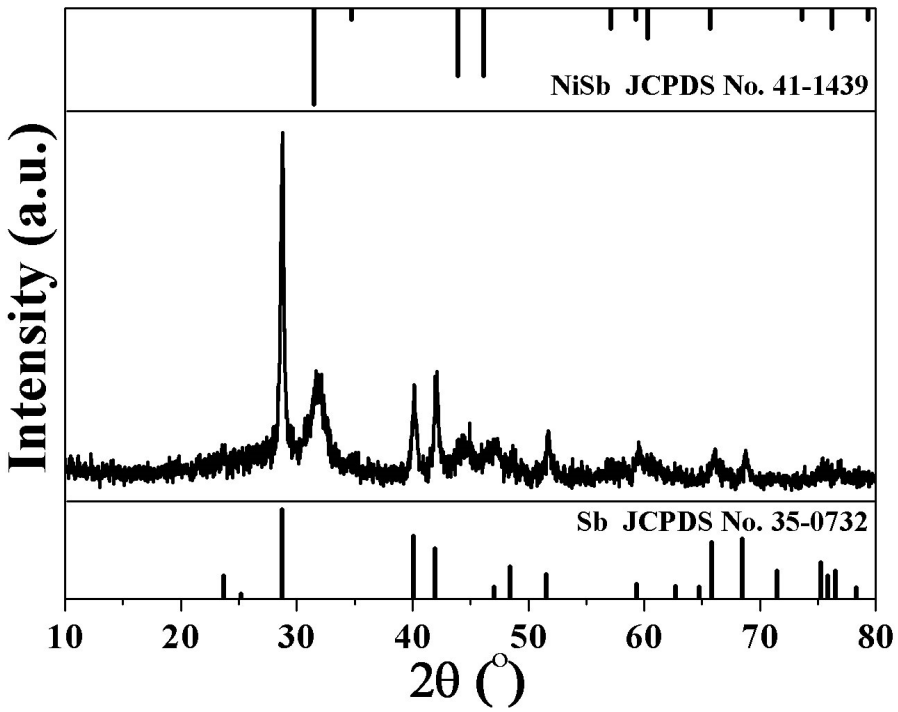

Figure S1 XRD pattern of the Sb–Ni framework.

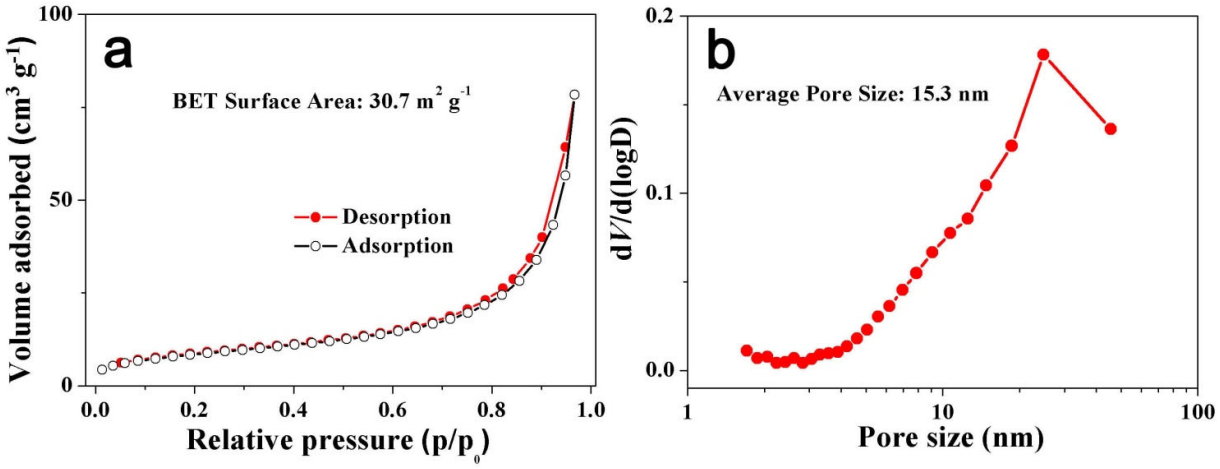

Figure S2 Nitrogen adsorption/desorption isotherms (a) and pore size distribution from the desorption branch (b) of the Sb–Ni framework material.

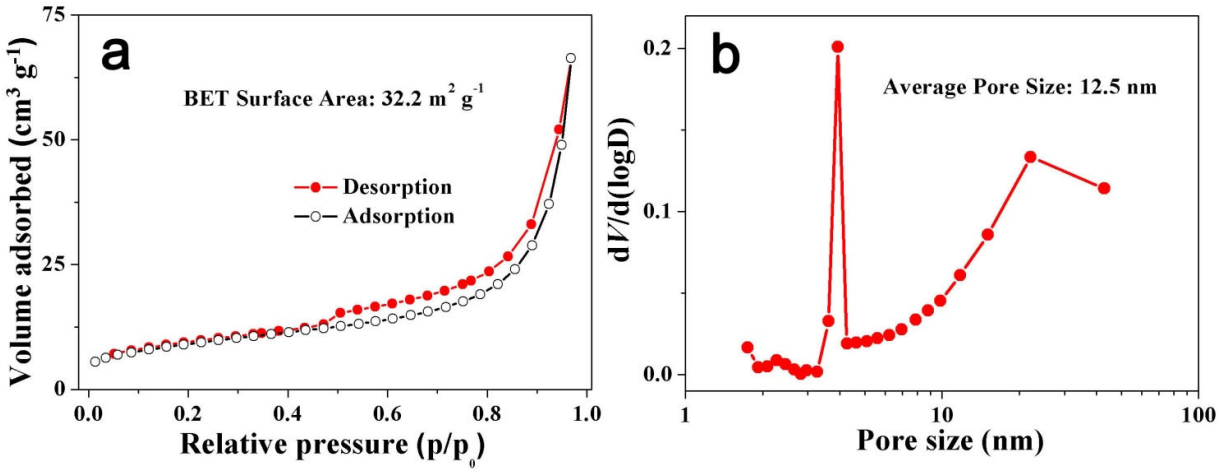

Figure S3 Nitrogen adsorption/desorption isotherms (a) and pore size distribution from the desorption branch (b) of the rGO@Sb–Ni ternary framework.

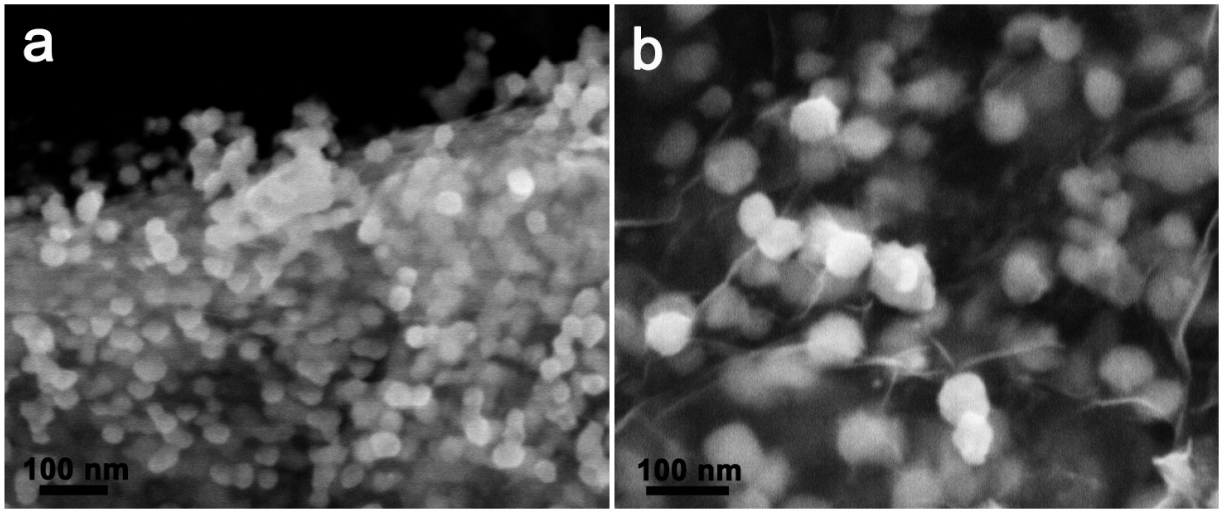

Figure S4 SEM images of the rGO@Sb–Ni framework.

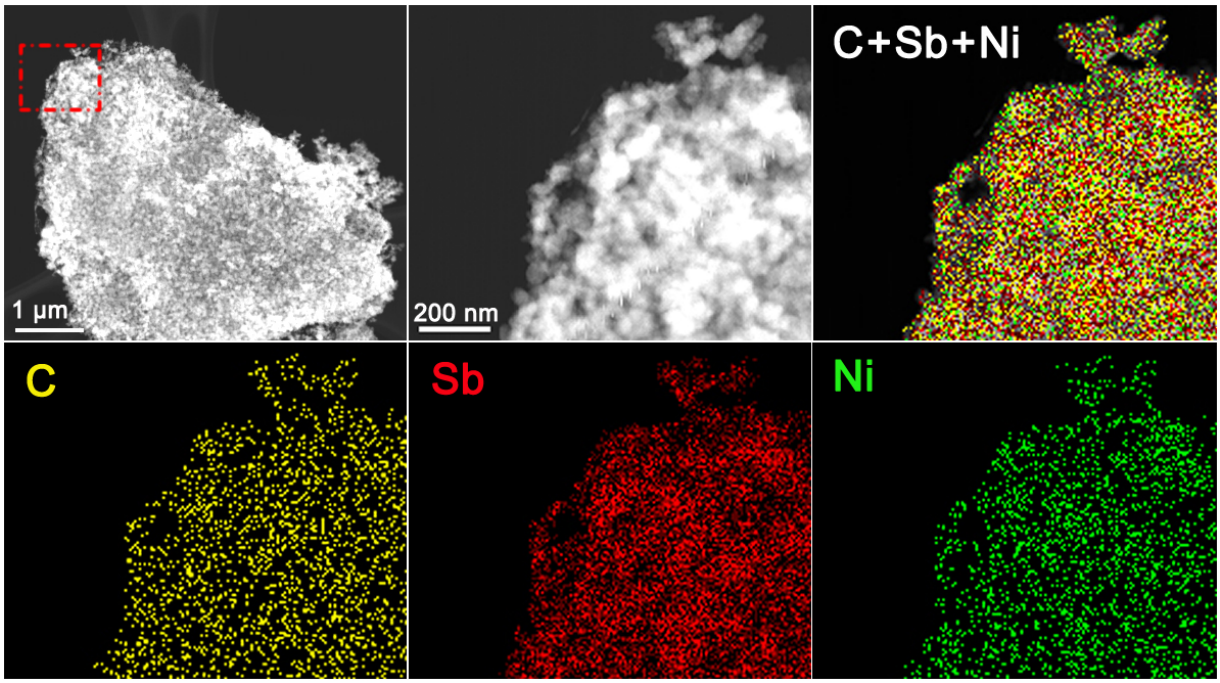

Figure S5 STEM-EDX elemental mappings of the rGO@Sb–Ni framework.

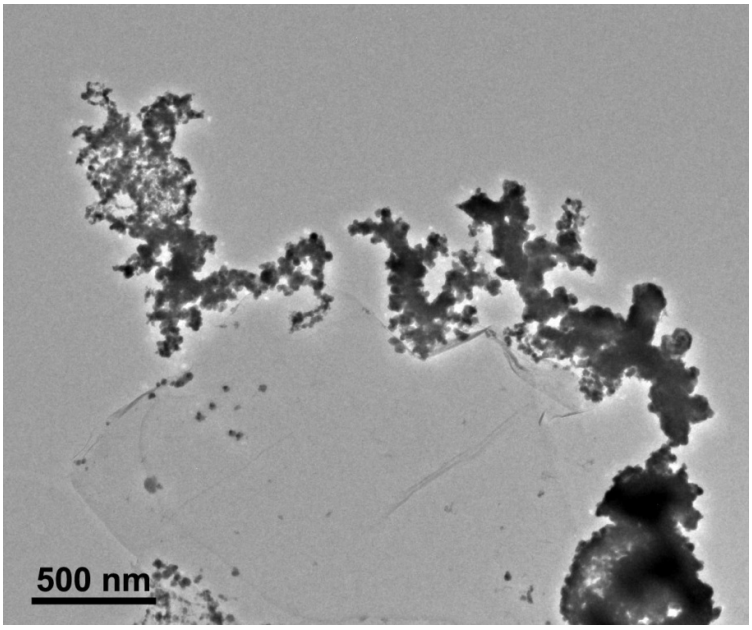

Figure S6 TEM image of the rGO–Sb–Ni composite prepared using $NiCl_2$ instead of $K_2Ni(CN)_4$ with other conditions unchanged.

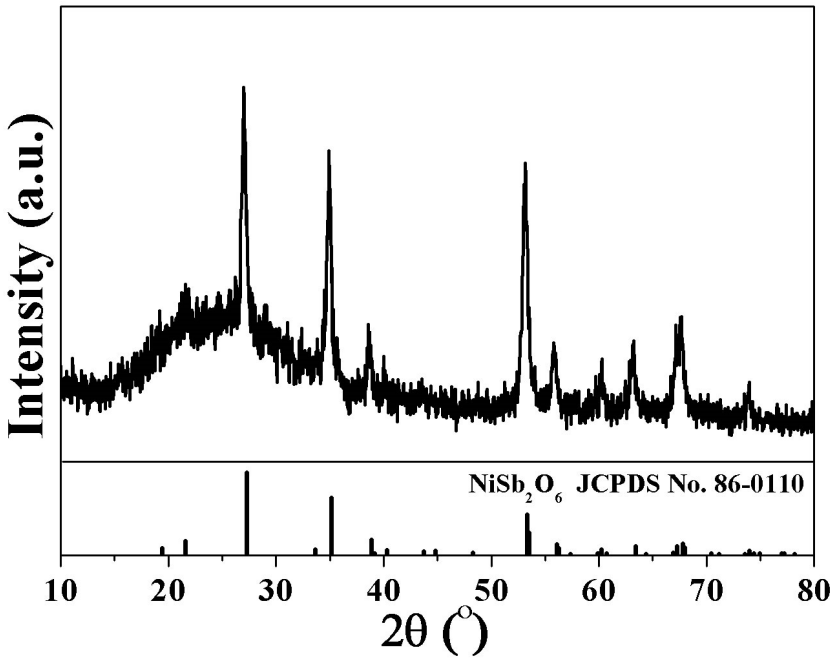

Figure S7 XRD pattern of the rGO@Sb–Ni framework after TGA.

As seen from TGA curves (Figure 3f), the weight variation of rGO@Sb–Ni frameworks can be mainly attributed to the oxidation of Sb–Ni alloy and rGO components during TGA tests. The oxidation of Sb–Ni alloy leads to a weight increase, while the removal of rGO leads to a weight decrease of the products. Figure S7 shows the XRD pattern of the rGO@Sb–Ni framework after TGA. The observed crystalline phase can be indexed to tetragonal $NiSb_2O_6$ (JCPDS no. 86-0110), in agreement with the feeding ratios of $SbCl_3$ and $K_2Ni(CN)_4$ reactants (molar ratio of Sb:Ni is 2:1). Thus, the rGO contents in these ternary frameworks can be calculated to be 26 wt% (20GO), 33 wt% (40GO), and 45 wt% (80GO), respectively, based on the following equation:

$$\begin{aligned} \text{rGO(wt\%)} &= 100 - \text{Sb-Ni(wt\%)} \\ &= 100 - 100 \times \frac{\text{molecular weight of 2Sb and Ni}}{\text{molecular weight of } NiSb_2O_6} \times \frac{\text{final weight of } NiSb_2O_6}{\text{initial weight of rGO@Sb-Ni}} \end{aligned}$$

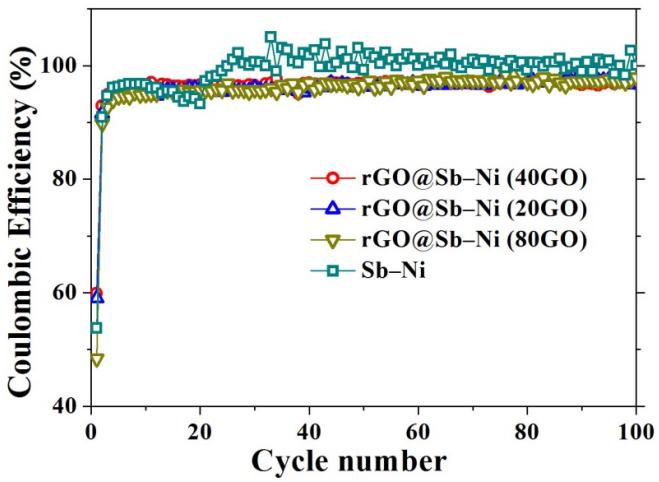

Figure S8 Coulombic efficiencies *versus* cycle numbers for the rGO@Sb–Ni and Sb–Ni frameworks.

The Coulombic efficiencies of the rGO@Sb–Ni and Sb–Ni frameworks have been demonstrated (Figure S8). As can be seen, the initial Coulombic efficiency of the rGO@Sb–Ni (40GO) framework is 60%, higher than those of rGO@Sb–Ni (20GO) (59%), rGO@Sb–Ni (80GO) (49%), and Sb–Ni (54%) frameworks. Their initial capacity loss is mainly due to the irreversible formation of solid electrolyte interface (SEI) layer ($Na^+ + e^- +$ electrolyte $\rightarrow$ SEI layer). Additionally, the average Coulombic efficiency of the optimal rGO@Sb–Ni (40GO) sample is 96.7% from 2 to 100 cycles, higher than those of rGO@Sb–Ni (20GO) (96.3%) and rGO@Sb–Ni (80GO) (96.4%) samples.

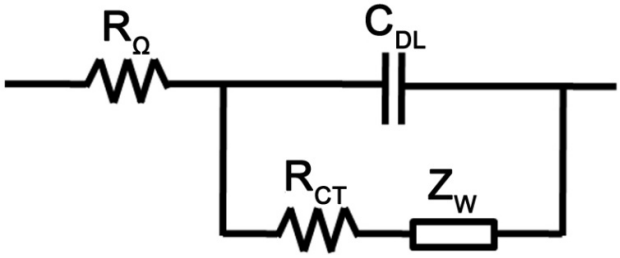

Figure S9 The equivalent circuit model for the fitting of impedance plots.

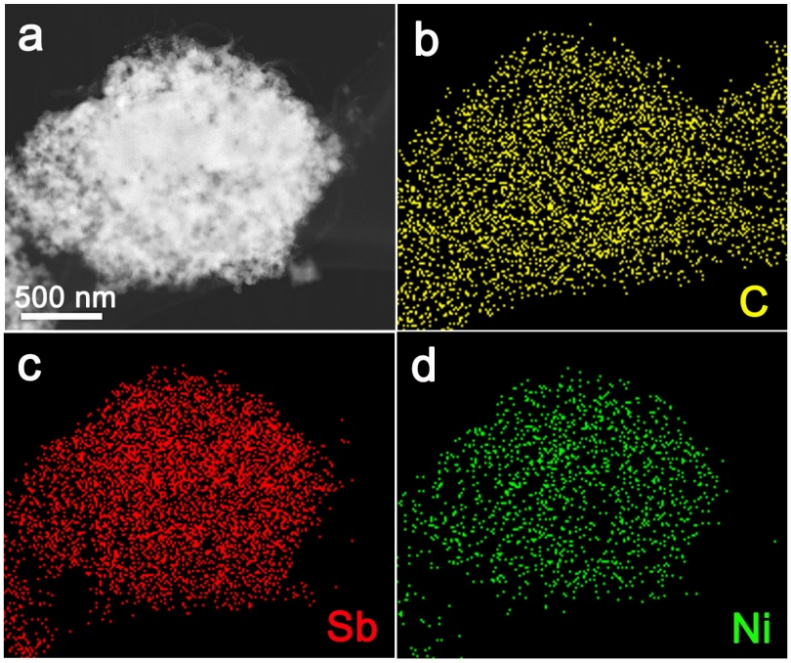

Figure S10 STEM-EDX elemental mapping of the CNT@Sb–Ni framework.

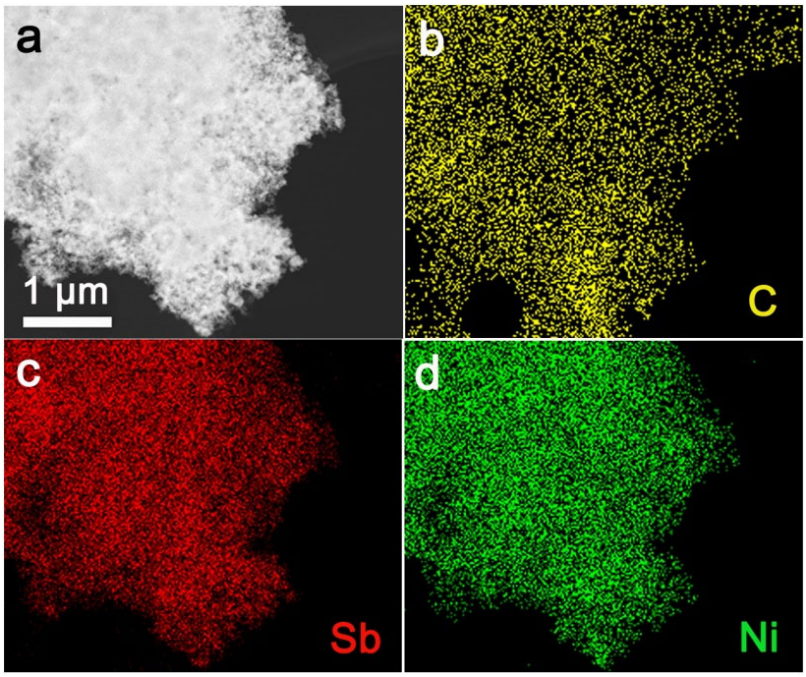

Figure S11 STEM-EDX elemental mapping of the CB@Sb–Ni framework.

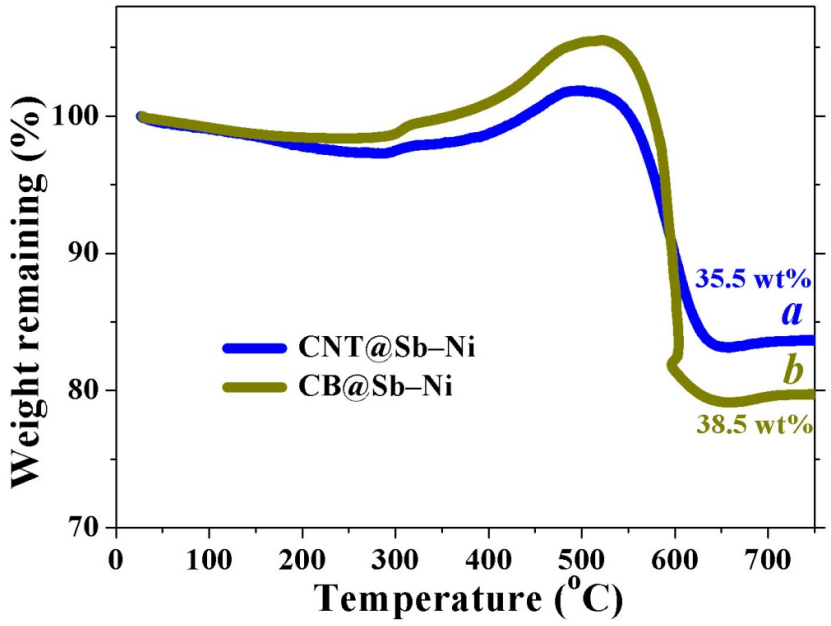

Figure S12 TGA curves of the CNT@Sb–Ni (curve *a*) and CB@Sb–Ni (curve *b*) framework materials.

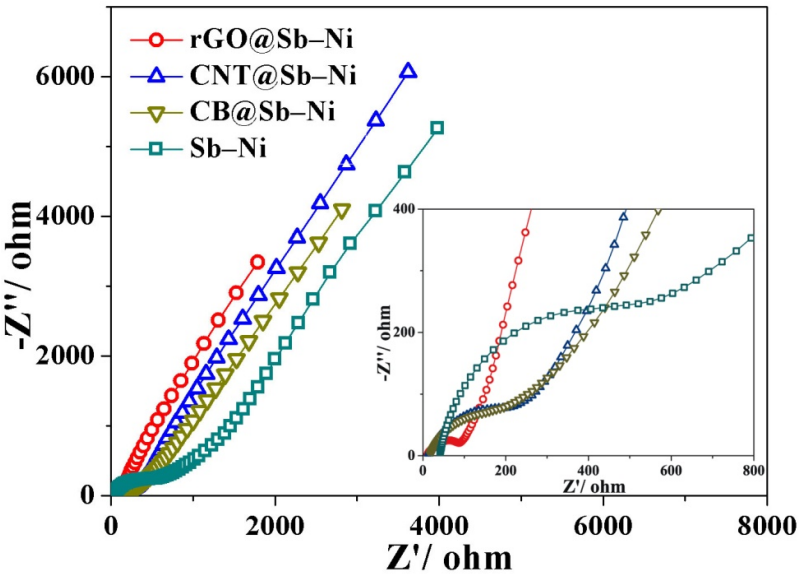

Figure S13 Nyquist plots of the rGO@Sb–Ni, CNT@Sb–Ni, CB@Sb–Ni, and bare Sb–Ni frameworks after the first cycle at a charged state (2.5 V *vs.* Na^+/Na).

Table S1. Comparison of the sodium storage performance between the rGO@Sb–Ni framework electrode and previously reported Sb-based anodes prepared by integrating Sb with transition-metals and/or carbon additives (CB, CNT, and graphene).

Active materials	Cycling stability ($mAh\ g^{-1}$)	Rate capability ($mAh\ g^{-1}$)	Ref
rGO@Sb–Ni network	463 at 100 mA g^{-1} (100 cycles) 210 at 5000 mA g^{-1} (500 cycles)	~530 at 200 mA g^{-1} ~498 at 500 mA g^{-1} ~468 at 1000 mA g^{-1}	This work
3-D Sb/NiSb/Ni electrode	391 at 66 mA g^{-1} (300 cycles)		1
3D interconnected NiSb hollow nanospheres	500 at 60 mA g^{-1} (70 cycles) 230 at 6000 mA g^{-1} (150 cycles)	~500 at 120 mA g^{-1} ~400 at 600 mA g^{-1}	2
Cu_2Sb/Cu electrode	270 at 800 mA g^{-1} (200 cycles)	288.2 at 200 mA g^{-1} 267.9 at 2000 mA g^{-1}	3
$FeSb_2$ electrode	440 at 300 mA g^{-1} (130 cycles)	~515 at 72 mA g^{-1} ~490 at 300 mA g^{-1}	4
Sb/acetylene black composite	473 at 100 mA g^{-1} (70 cycles)	420 at 200 mA g^{-1} 281 at 800 mA g^{-1}	5
Sb/MWCNT nanocomposite	~400 at 200 mA g^{-1} (120 cycles)	449 at 200 mA g^{-1} 401 at 500 mA g^{-1} 350 at 1000 mA g^{-1}	6
Sb/multilayer graphene hybrid	406 at 100 mA g^{-1} (200 cycles)	456 at 200 mA g^{-1} 428 at 500 mA g^{-1} 382 at 1000 mA g^{-1}	7
I-Sb/rGO nanocomposite	173 at 500 mA g^{-1} (150 cycles)	243 at 200 mA g^{-1} 213 at 500 mA g^{-1} 188 at 1000 mA g^{-1}	8
G@NiSb/Sb@Ni-foam	305 at 300 mA g^{-1} (100 cycles)	435 at 200 mA g^{-1} 371 at 500 mA g^{-1} 315 at 1000 mA g^{-1}	9
Cu_2Sb–Al_2O_3–C	~200 at 100 mA g^{-1} (70 cycles)	230 at 500 mA g^{-1} 215 at 1000 mA g^{-1}	10
FeSb–TiC–C nanocomposite	210 at 100 mA g^{-1} (60 cycles)	~190 at 500 mA g^{-1} ~184 at 1000 mA g^{-1}	11

Table S2. The fitting results of R_{Ω} and R_{CT} (Ω) of the rGO@Sb–Ni networks and Sb–Ni networks from EIS tests.

	rGO@Sb–Ni (40GO)	rGO@Sb–Ni (20GO)	rGO@Sb–Ni (80GO)	Sb–Ni
R_{Ω}	13.2	16.3	14.4	44.8
R_{CT}	33.4	65.1	46.5	333.3

Table S3. The fitting results of R_{Ω} and R_{CT} (Ω) of the rGO@Sb–Ni network in comparison with CNT@Sb–Ni, CB@Sb–Ni, and Sb–Ni networks from EIS tests.

	rGO@Sb–Ni	CNT@Sb–Ni	CB@Sb–Ni	Sb–Ni
R_{Ω}	13.2	17.5	23.5	44.8
R_{CT}	33.4	93.7	108.2	333.3

References

(1) Lee, C. W.; Kim, J. C.; Park, S.; Song, H. J.; Kim, D. W. Highly Stable Sodium Storage in 3-D Gradational Sb–NiSb–Ni Heterostructures. *Nano Energy* **2015**, *15*, 479–489.

(2) Liu, J.; Yang, Z.; Wang, J.; Gu, L.; Maier, J.; Yu, Y. Three-Dimensionally Interconnected Nickel–Antimony Intermetallic Hollow Nanospheres as Anode Material for High-Rate Sodium-Ion Batteries. *Nano Energy* **2015**, *16*, 389–398.

(3) Wang, L. B.; Wang, C.; Zhang, N.; Li, F.; Cheng, F.; Chen, J. High Anode Performance of in Situ Formed Cu_2Sb Nanoparticles Integrated on Cu Foil via Replacement Reaction for Sodium-Ion Batteries. *ACS Energy Lett.* **2017**, *2*, 256–262.

(4) Darwiche, A.; Toiron, M.; Sougrati, M. T.; Fraisse, B.; Stievano, L.; Monconduit, L. Performance and Mechanism of $FeSb_2$ as Negative Electrode for Na-Ion Batteries. *J. Power Sources* **2015**, *280*, 588–592.

(5) Hou, H.; Yang, Y.; Zhu, Y.; Jing, M.; Pan, C.; Fang, L.; Song, W.; Yang, X.; Ji, X. An Electrochemical Study of Sb/Acetylene Black Composite as Anode for Sodium-Ion Batteries. *Electrochim. Acta* **2014**, 146, 328–334.

(6) Zhou, X.; Dai, Z.; Bao, J.; Guo, Y. G. Wet Milled Synthesis of an Sb/MWCNT Nanocomposite for Improved Sodium Storage. *J. Mater. Chem. A* **2013**, *1*, 13727–13731.

(7) Hu, L.; Zhu, X.; Du, Y.; Li, Y.; Zhou, X.; Bao, J. A Chemically Coupled Antimony/Multilayer Graphene Hybrid as a High-Performance Anode for Sodium-Ion Batteries. *Chem. Mater.* **2015**, *27*, 8138–8145.

(8) Wan, F.; Lu, H. Y.; Zhang, X. H.; Liu, D. H.; Zhang, J. P.; He, X.; Wu, X. L. The in-Situ-Prepared Micro/Nanocomposite Composed of Sb and Reduced Graphene Oxide as Superior Anode for Sodium-Ion Batteries. *J. Alloys Compd.* **2016**, *672*, 72–78.

(9) Ding, Y. L.; Wu, C.; Kopold, P.; van Aken, P. A.; Maier, J.; Yu, Y. Graphene-Protected 3D Sb-based Anodes Fabricated via Electrostatic Assembly and Confinement Replacement for Enhanced Lithium and Sodium Storage. *Small* **2015**, *11*, 6026–6035.

(10) Kim, I. T.; Allcorn, E.; Manthiram, A. High-Performance M_xSb–Al_2O_3–C (M=Fe, Ni, and Cu) Nanocomposite-Alloy Anodes for Sodium-Ion Batteries. *Energy Technol.* **2013**, *1*, 319–326.

(11) Kim, I. T.; Allcorn, E.; Manthiram, A. High-Performance FeSb–TiC–C Nanocomposite Anodes for Sodium-Ion Batteries. *Phys. Chem. Chem. Phys.* **2014**, *16*, 12884–12889.